THE JOURNAL OF BIOLOGICAL CHEMISTRY VOL. 286, NO. 28, pp. 25363–25376, July 15, 2011

Regulation of Purinergic Signaling in Biliary Epithelial Cells by Exocytosis of SLC17A9-dependent ATP-enriched Vesicles*[S]

Received for publication, February 18, 2011, and in revised form, May 12, 2011 Published, JBC Papers in Press, May 25, 2011, DOI 10.1074/jbc.M111.232868

Meghana N. Sathe[‡], Kangmee Woo[‡], Charles Kresge[‡], Abhijit Bugde[§], Kate Luby-Phelps[§], Matthew A. Lewis[¶], and Andrew P. Feranchak[‡1]

From the Departments of [‡]Pediatrics, [§]Cell Biology, and [¶]Radiology, University of Texas Southwestern Medical Center, Dallas, Texas 75390

ATP in bile is a potent secretogogue, stimulating biliary epithelial cell (BEC) secretion through binding apical purinergic receptors. In response to mechanosensitive stimuli, BECs release ATP into bile, although the cellular basis of ATP release is unknown. The aims of this study in human and mouse BECs were to determine whether ATP release occurs via exocytosis of ATP-enriched vesicles and to elucidate the potential role of the vesicular nucleotide transporter SLC17A9 in purinergic signaling. Dynamic, multiscale, live cell imaging (confocal and total internal reflection fluorescence microscopy and a luminescence detection system with a high sensitivity charge-coupled device camera) was utilized to detect vesicular ATP release from cell populations, single cells, and the submembrane space of a single cell. In response to increases in cell volume, BECs release ATP, which was dependent on intact microtubules and vesicular trafficking pathways. ATP release occurred as stochastic point source bursts of luminescence consistent with exocytic events. Parallel studies identified ATP-enriched vesicles ranging in size from 0.4 to 1 μm that underwent fusion and release in response to increases in cell volume in a protein kinase C-dependent manner. Present in all models, SLC17A9 contributed to ATP vesicle formation and regulated ATP release. The findings are consistent with the existence of an SLC17A9-dependent ATP-enriched vesicular pool in biliary epithelium that undergoes regulated exocytosis to initiate purinergic signaling.

Purinergic signaling has emerged as a dominant pathway regulating biliary secretion and bile formation. Released into bile by both hepatocytes and biliary epithelial cells (known as cholangiocytes) in response to mechanosensitive stimuli (cell swelling and flow/shear stress) (1–3), extracellular ATP activates P2 receptors in the apical membrane of targeted cholangiocytes, resulting in increases in $[Ca^{2+}]_i$, activation of K^+ (4, 5) and Cl^- (6, 7) channels, and a robust secretory response (8). Recent studies suggest that even the classical model of biliary epithelial cell secretion wherein secretin stimulates Cl^- secretion via increases in cAMP is mediated by a pathway regulated by ATP release and autocrine/paracrine stimulation of P2 receptors on the apical cholangiocyte membrane (9, 10).

The cellular mechanism of biliary epithelial ATP release has not been identified. Two potential pathways exist: transporter/channel-mediated or exocytosis of ATP-containing vesicles. Cholangiocytes express several ATP-binding cassette proteins, such as MDR-1 and the cystic fibrosis transmembrane conductance regulator (CFTR)[2] (11, 12), implicated in ATP release. However, the effect of MDR-1 on ATP release can be disassociated from p-glycoprotein-related substrate transport, suggesting that MDR-1 *per se* is not likely to function as an ATP channel (13). Similarly, despite provocative data that CFTR functions as a regulator of ATP release, many cells exhibit ATP release in the absence of apparent CFTR expression, including hepatocytes (1, 14), and no evidence of a CFTR-mediated ATP conductance could be demonstrated in other models (15, 16).

Conversely, studies in biliary epithelium demonstrate that stimuli that increase the rate of exocytosis (*e.g.* cell volume increases and cAMP) are associated with parallel increases in ATP release (17). Additionally, volume-stimulated biliary epithelial cell ATP release is regulated by phosphoinositide 3-kinase (PI3K) (18) and protein kinase C (PKC) (3, 17, 19), kinases associated with vesicular trafficking. Furthermore, substantial evidence has emerged to indicate that vesicular exocytosis contributes to ATP release in other models (20–23), and we have recently identified an ATP-enriched vesicle pool in liver cells that undergoes microtubule-dependent trafficking and release in response to increases in cell volume (24). The identification of a vesicular nucleotide transporter, SLC17A9, responsible for loading ATP into vesicles (25) provides further evidence that exocytosis of ATP-containing vesicles initiates purinergic signaling in some cells (25–27). However, the expression and/or function of SLC17A9 in biliary epithelium is unknown.

The aim of our studies therefore was to elucidate the cellular basis of and the potential role of SLC17A9 in biliary cell ATP release. Studies were performed utilizing dynamic imaging modalities of live human and mouse biliary cells at different scales, including confluent cell populations, single cells, and the intracellular submembrane space of a single cell. The findings are consistent with the existence of an SLC17A9-dependent

* This work was supported, in whole or in part, by National Institutes of Health Grant DK078587 from the NIDDK (to A. P. F.). This work was also supported by Cystic Fibrosis Foundation Grant FERANC08G0 and the Children's Medical Center Foundation (to A. P. F.).

[S] The on-line version of this article (available at http://www.jbc.org) contains supplemental Table S1 and Figs. S1–S4.

[1] To whom correspondence should be addressed: Dept. of Pediatrics, University of Texas Southwestern Medical Center, 5323 Harry Hines Blvd., Dallas, TX 75390-9063. Tel.: 214-648-2386; Fax: 214-648-2673; E-mail: drew.feranchak@utsouthwestern.edu.

[2] The abbreviations used are: CFTR, cystic fibrosis transmembrane conductance regulator; BEC, biliary epithelial cell; CCD, charge-coupled device; MLC, mouse large cholangiocyte; MSC, mouse small cholangiocyte; L-L, luciferin-luciferase; ALU, arbitrary light unit; TIRF, total internal reflection fluorescence; PMA, phorbol 12-myristate 13-acetate.

ATP-enriched vesicular pool in biliary epithelium that undergoes regulated exocytosis in response to increases in cell volume.

EXPERIMENTAL PROCEDURES

Cell Models—Human Mz-Cha-1 biliary cells (28) and mouse large (MLCs) and small (MSCs) cholangiocytes (29) derived from large and small intrahepatic bile ducts, respectively, and transformed via SV40 transfection were cultured as described previously (7, 30). Each model system expresses phenotypic features of differentiated biliary epithelium, including receptors, signaling pathways, and ion channels, similar to those found in primary cells (7, 29, 30). Unlike Mz-Cha-1 cells, MLCs and MSCs form polarized monolayers with intercellular tight junctions and apical microvilli (30). Although both MSCs and MLCs express a full repertoire of P2 receptors and exhibit Ca^{2+}-stimulated secretion in response to ATP (30), only MLCs express CFTR (29). Cells were grown on 35-mm dishes for 2–4 days in preparation for bioluminescence studies. For confocal microscopy studies, cultured cells were plated in eight-chamber coverglass slides (Nalge Nunc Lab-Tek chambered coverglasses (8-well), Fisher catalogue number 12-565-470) 1–2 days prior to experiment.

Bulk ATP Release by Luminometric Assay—Bulk ATP release was studied from confluent cells using the luciferin-luciferase (L-L) assay as described previously (31). Cells were grown to confluence on 35-mm tissue culture-treated dishes (Falcon, BD Biosciences Discovery Labware) and washed with PBS (600 μl × 2), 600 μl of Opti-MEM (Invitrogen) containing L-L (FL-ATP Assay Mix (Sigma-Aldrich) reconstituted according to the manufacturer's directions and used at a final dilution of 1:50 with Opti-MEM) were added, and then cells were placed into a modified Turner TD 20/20 luminometer in complete darkness. After a 5–10-min equilibration period, readings were obtained every 15 s, and cumulative bioluminescence over 15-s photon intervals was quantified in real time as arbitrary light units (ALUs). Studies were performed at room temperature as luciferase activity decreases at higher temperatures. ATP standard curves were generated to approximate ATP concentrations by measuring luminescence after adding dilutions of a freshly prepared stock solution of ATP to the luciferin-luciferase assay mixture as described above.

ATP Release by Point Source Chemiluminescence Assay—Point source ATP release was detected from confluent cells as described previously (24). Briefly, cells were grown to confluence on 35-mm tissue culture-treated dishes, medium was removed, cells were washed with PBS, L-L (1:25 dilution) was added, cells were placed in a light-tight box with an optical imaging apparatus, and the box was attached to a perfusion system (Pump 33, Harvard Apparatus, Holliston, MA). Light produced by the catalysis of the L-L reaction by released ATP was detected by a high sensitivity electron-multiplying CCD camera (Princeton Instruments/ACTON PhotonMAX 512B with the e2v CCD97 sensor, 512 × 512 pixels) mounted in a vertical orientation on an x-y-z stage. A relay lens consisting of two 25.4-mm format lenses (Schneider xenon f/0.95) coupled front to front with each focused at infinity with full aperture was used to image at 1×. Images were collected at a frequency of 9–10 Hz with 100-ms exposure time during basal (isotonic) and hypotonic conditions. Typical stacks of 500–700 images were streamed to hard disk for storage and data analysis. Full electron multiplication stage gain was utilized in all experiments for maximum sensitivity. Base-line image stacks prior to hypotonic stimulation were also obtained for residual ATP detection and electron multiplication noise characterization. Precautions were taken to avoid overexposure of the high gain sensor mode as this has been shown to reduce sensitivity.

Lactate Dehydrogenase Release—Lactate dehydrogenase measurements were performed pre- and posthypotonic exposure using an enzymatic colorimetric cytotoxicity assay (CytoTox 96, Promega, Madison, WI). Calibration of the assay was performed with cell-free controls and reagents only (no lactate dehydrogenase release), with lactate dehydrogenase standard at a dilution of 1:5000 (amount of lactate dehydrogenase in ~13,000 lysed cells), and after exposure of cells to lysis solution (maximum lactate dehydrogenase release).

ATP-enriched Vesicle Staining—Quinacrine (Sigma), an acridine derivative, has a very high affinity for ATP and has been utilized to label intracellular ATP-enriched vesicles in other cell types (21, 23, 32–34). Cells cultured on a Lab-Tek glass bottom 8-well imaging coverglass (Nalge Nunc, Rochester, NY) were washed with PBS and stained with quinacrine (5 μM × 5 min), washed, and placed in isotonic buffer. In select studies, FM4-64 (4 μM × 10–45 min; Invitrogen/Molecular Probes) used to label the plasma membrane and endocytic vesicles preceded or accompanied quinacrine staining.

Confocal Imaging—Cells were cultured on a Lab-Tek 8-well chambered coverglass (Nalge Nunc), labeled with FM4-64 and quinacrine, and imaged under basal and hypotonic conditions as described above. Imaging was performed using a Perkin-Elmer UltraVIEW ERS spinning disk confocal microscope (PerkinElmer Life Sciences). An argon ion laser and a krypton laser (CVI Melles Griot, Carlsbad, CA) were utilized as a light source (excitation, 488 and 561 nm, respectively), and data were captured with a Hamamatsu ORCA-AG high resolution cooled CCD camera (Hamamatsu, Bridgewater, NJ) controlled by the UltraVIEW ERS software. Images were recorded using a Zeiss Plan Apo 63×/1.40 numerical aperture oil immersion objective lens. Fast multicolor images were captured using emission band pass filters to allow effective separation of overlapping wavelengths, and 2 × 2 binning was selected for all images. The speed of acquisition was increased by subarraying the camera to reduce the size of the captured image. Image analysis was performed utilizing NIH ImageJ, and Imaris 5.0–6.2 (Bitplane Inc., Saint Paul, MN) was used for three-dimensional volume rendering of z-stacks after background correction and edge-enhancing anisotropic diffusion filtering. The Imaris spot detection algorithm was applied to detect and measure objects (vesicles) after specifying minimum diameter so that speckle noise was not detected. We defined small vesicles as those between 0.4 and 0.99 μm and large vesicles as those ≥1 μm. Potential co-localization between FM4-64- and quinacrine-labeled vesicles was evaluated by application of Imaris 5.0–6.2 utilizing the co-localization feature with complete (100%) co-localization indicated by a Pearson's coefficient ≥1.00.

Total Internal Reflection Fluorescence (TIRF) Imaging—Cells were cultured on a Lab-Tek 8-well chambered coverglass (Nalge Nunc), stained with quinacrine, and imaged under basal and hypotonic conditions as described above. TIRF imaging was performed on an Olympus IX71 microscope equipped with an Olympus TIRF module. Quinacrine TIRF was excited with the 488-nm line of a 10-milliwatt argon laser (CVI Melles Griot) through a 60× PlanApo-N 1.45 numerical aperture oil immersion lens or a PLAPO 100× 1.45 numerical aperture TIRFM oil immersion lens as described (35). Laser intensity was modulated by neutral density filters and Uniblitz electronic shutters (Vincent Associates, Rochester, NY). Time lapse images were acquired every 300 ms with exposure times of 100–200 ms using SlideBook (Intelligent Imaging Innovations, Inc., Denver, CO) to control a Hamamatsu Orca II ERG camera (Hamamatsu Photonics) and the electronic shutters.

Detection of SLC17A9—Total RNA was extracted using QIAshredder and RNeasy minikit (Qiagen, Valencia, CA). Purified RNA (2 μg) was converted to cDNA with a SuperScript III First Strand kit (Invitrogen) in the presence of oligo(dT) primers according to the manufacturer's directions. RT-PCR was performed using a PerkinElmer Life Sciences PCR system (94 °C, 30 s; 57.5 °C, 30 s; 72 °C, 30 s; 40 cycles) after initial denaturation at 94 °C for 5 min using *Taq* polymerase (Invitrogen). The primers used for RT-PCR are shown in supplemental Table S1 (27). Expression was normalized with human GAPDH for Mz-Cha-1 and murine β-actin for MSCs and MLCs. Signals were visualized via enhanced chemiluminescence detection (Pierce) and captured with a digital image system (Chemigenius2 photodocumentation system, Syngene, Cambridge, UK).

SLC17A9 Silencing—SLC17A9 was suppressed by human SLC17A9 siRNA designed and synthesized by Santa Cruz Biotechnology (catalogue number sc-72740). Non-coding Stealth™ RNAi (medium GC duplex; Invitrogen) was utilized in control (mock) transfections. BLOCK-iT™ Fluorescent Oligo (Invitrogen catalogue number 2013) was used to optimize transfection conditions. Briefly, cells were washed with PBS and incubated in 500 μl of Opti-MEM containing siRNA (final concentration, 100 nM) and FuGENE reagent (Roche Applied Science) for 2 h at 37 °C in a CO_2 incubator. After 2 h, the supernatant was removed, and cell culture medium was added for a 48-h incubation. Quantitative assessment was determined by real time PCR using the 7900HT Fast Real-Time PCR system (Applied Biosystems/Invitrogen). The primers for human SLC17A9 are: forward, 5′-cgctggtctatgatctttgcgtcagcg-3′; reverse, 5′-ggccaggtcctgaatgttgact-3′. Reactions were performed in quadruplicate using the SYBR Green Supermix (Bio-Rad) according to the manufacturer's recommendations. Quantification of SLC17A9 expression was normalized to hGAPDH expression.

Reagents—All of the reagents were obtained from Sigma-Aldrich. None of the reagents affected L-L luminescence as measured during cell-free conditions.

Statistics—Results are presented as the means ± S.E. with n representing the number of culture plates or repetitions for each assay as indicated. Statistical analysis included Fisher's paired and unpaired t test and analysis of variance for multiple comparisons to assess statistical significance as indicated, and p values <0.05 were considered to be statistically significant.

RESULTS

Inhibitors of Vesicular Trafficking Block ATP Release from Biliary Cells—Bulk ATP release was measured in Mz-Cha-1 cells and MSC and MLC monolayers in the presence or absence of pharmacologic inhibitors of vesicular formation or trafficking. It should be noted that MSCs do not express CFTR (29), excluding CFTR as a potential mechanism of volume-stimulated ATP release in these cells. Under basal (isotonic) conditions, luminescence was detected in all biliary epithelial preparations, reflecting constitutive ATP release (Fig. 1 and supplemental Fig. S4). Addition of a small volume (200 μl) of isotonic buffer resulted in a small but significant increase in ATP release in all preparations, reflecting ATP release secondary to mechanical stimulation (14). Exposure to an equal volume of hypotonic buffer (33% dilution) to increase cell volume resulted in a dramatic increase in ATP released into bulk solution (to ~135 ± 15 nM). MSC and MLC monolayers also exhibited significant volume-stimulated ATP release (Fig. 1, *B* and *C*). In contrast, incubation with brefeldin A, an inhibitor of protein translocation through the Golgi (22), significantly inhibited volume-stimulated ATP release in all biliary models. In separate studies, incubation with nocodazole, a microtubule-depolymerizing agent, had a similar inhibitory effect on volume-stimulated ATP release. Together, the findings demonstrate that intact vesicular formation and trafficking pathways are required for volume-stimulated ATP release from human and mouse biliary cells.

Identification of Point source Bursts of ATP Release from Confluent Biliary Cells—Although the above studies reflect bulk measurements of ATP in solution, we sought to determine whether localized "points" of ATP release could be observed, suggesting distinct exocytic events of individual cells as recently described for cultured liver cells (24). For these studies, confluent cells were perfused with luciferin-luciferase-containing medium, maintained in a dark environment, and imaged with a high sensitivity electron-multiplying CCD camera. Under these conditions, the appearance of ATP in the medium was detected in real time by light emissions resulting from ATP-dependent luciferase-catalyzed oxidation of luciferin (24). A representative sequence of images from a confluent monolayer of MSC cells is shown in Fig. 2 (real time movie is shown in supplemental Fig. S1). Under basal conditions, there was low background activity. Decreasing medium osmolality (by 33%) to produce an increase in cell volume resulted in an increase in luminescence that was focused as distinct point source bursts of high intensity. Each burst reached maximal intensity within 2 s and then decayed rapidly (Fig. 2*B*). The maximal diameter of an individual burst was 312 ± 24 μm (n = 45; represented in Fig. 2*B*, *inset*). ATP release was restricted to single events, and no subsequent events at the same site were noted. There were no associated release of lactate dehydrogenase and no evidence of cell injury or necrosis when visualized by conventional microscopy (not shown). MLC monolayers and Mz-Cha-1 cells exhibited a similar stochastic pattern of point source ATP release (supplemental Fig. S2). There was no difference in the number of events or the maximal diffusion size of individual bursts between biliary cell types (Table 1). In the

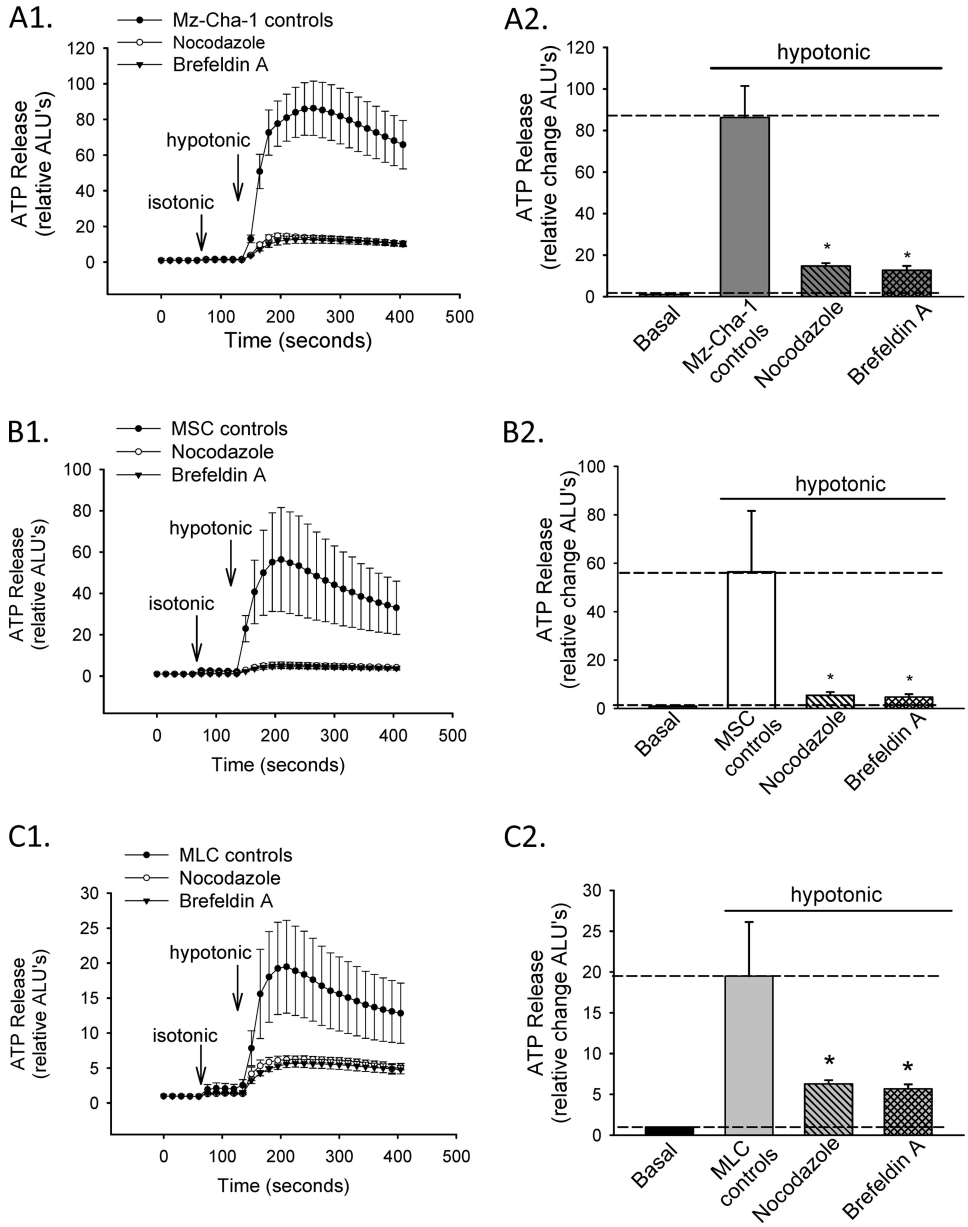

FIGURE 1. **Effects of pharmacologic inhibition of vesicle formation (brefeldin A) and trafficking (nocodazole) on volume-stimulated ATP release.** ATP release from confluent Mz-Cha-1 (*A1* and *A2*), MSC (*B1* and *B2*), and MLC (*C1* and *C2*) cells was detected using a luciferin-luciferase assay and recorded as relative ALUs (*y axis*). *A1*, in control Mz-Cha-1 cells (●) addition of isotonic medium (*isotonic*; *arrow*) led to a small but significant increase in bioluminescence due to mechanical stimulation. Dilution of medium 33% by adding water to promote increases in cell volume (*hypotonic*; *arrow*) produced a larger increase in luminescence. Inhibition of vesicular formation with brefeldin A (10 μM × 2 h) (▼) or inhibition of microtubule polymerization with nocodazole (10 μM × 30 min) (○) significantly inhibited volume-stimulated ATP efflux. *A2*, cumulative data (mean ± S.E.) demonstrating effects of nocodazole ($n = 10$) and brefeldin ($n = 10$) on volume-stimulated ATP release *versus* control ($n = 20$; *, $p < 0.001$ for each). *B1* and *B2*, volume-stimulated ATP release in MSC monolayers in the presence or absence of nocodazole ($n = 6$) or brefeldin A ($n = 6$) utilizing a protocol identical to that described above for Mz-Cha-1 cells (*, $p < 0.01$ *versus* control; $n = 12$). *C1* and *C2*, volume-stimulated ATP release in MLC monolayers in the presence or absence of nocodazole ($n = 4$) or brefeldin A ($n = 4$) utilizing an identical protocol (*, $p < 0.01$ *versus* control; $n = 8$).

presence of high dose suramin (100 μM) to block P2 receptors, there was no difference in the number or size of ATP bursts compared with control cells, demonstrating that bursts were not due to ATP-stimulated ATP release from neighboring cells (regenerative ATP release). Thus, in both mouse and human biliary cells, volume-stimulated ATP release is not uniform but occurs as focal points of high intensity across a population of cells. Each event is discrete and non-recurring and produces a localized zone of increased ATP concentration that diffuses rapidly over a range corresponding to ~20 cell diameters.

Evidence for ATP-containing Vesicles—The stochastic, non-recurring, point source release of ATP is most compatible with a mechanism involving exocytosis of ATP-containing vesicles. In an effort to visualize candidate vesicles containing ATP, confluent cells were preincubated with quinacrine, which has a high affinity for ATP and produces a concentration-dependent fluorescence when exposed to blue light (21, 23, 32–34). Cells were secondarily stained with FM4-64 to label the plasma membrane and were assessed using digital reconstruction of spinning disk confocal z-stacks to quantify the location and

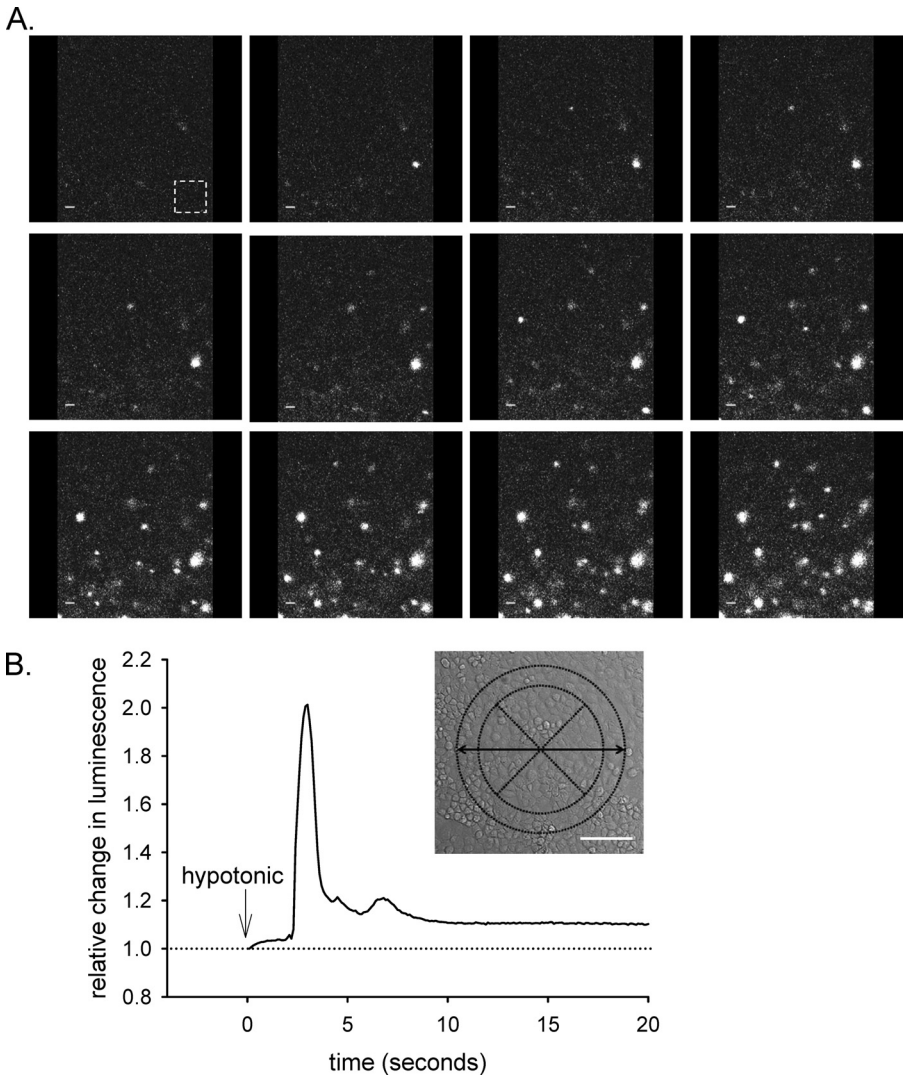

FIGURE 2. **Identification of point source bursts of ATP release from confluent biliary cells.** ATP release was detected from confluent MSC as focal increases in bioluminescence generated by ATP-dependent luciferin breakdown by luciferase (see supplemental Fig. S1 for point source ATP release). *A*, time lapse images of a representative study. Hypotonic solution was perfused onto confluent cells from a pipette immediately above the cells and to right of view. The first image was obtained 10 s after hypotonic addition, and sequential images (from *left* to *right* and *top* to *bottom*) represent 100-ms intervals. *Scale bar*, 100 μm. *B*, relative change in bioluminescence of one individual burst event. The *inset* represents a bright field image approximating the small square area outlined by *dotted lines* in the first frame. The maximal burst diameter (mean ± S.E.) was measured for 45 bursts and represented by the *double-headed arrow* in the *inset*. *Scale bar*, 100 μm.

TABLE 1

Comparison of point source burst events between biliary cell types

	Control		+Suramin (100 μm)	
	No. bursts/cm^2/min[a]	Burst diameter[b]	No. bursts/cm^2/min	Burst diameter
		μm		μm
MSC	84 ± 14, n = 10	312 ± 24, n = 45	79 ± 10, n = 6	297 ± 31, n = 14
MLC	75 ± 15, n = 8	288 ± 32, n = 30	70 ± 13, n = 4	315 ± 27, n = 12
Mz-Cha-1	82 ± 11, n = 8	327 ± 38, n = 35		

[a] Mean ± S.E.; n = number of monolayers.
[b] Average burst diameter reported as mean ± S.E.; n = number of bursts analyzed.

distribution of quinacrine and FM4-64 fluorescence. Representative MSC and MLC monolayers are shown in Fig. 3. Quinacrine-labeling of cellular ATP stores was not uniform but rather was detected as discrete foci 0.4–1.5 μm in diameter consistent with intracellular vesicles. Imaging the monolayers 90 s after exposure to hypotonic medium (33%) to increase cell volume resulted in a decrease in the total number of vesicles by 64 ± 8% in MSCs (n = 10, $p < 0.001$) and by 27 ± 10% in MLCs (n = 9, $p < 0.01$). Mz-Cha-1 cells exhibited a similar distribution of quinacrine vesicles that decreased upon volume stimulation (supplemental Fig. S3). Loss of quinacrine-stained vesicles was not due to photobleaching as cells exposed to the laser alone and imaged under identical conditions did not lose fluorescence. Similar to the point source ATP bursts described above, not all cells within the monolayer uniformly released ATP in response to hypotonic exposure (Fig. 3*B*). Approxi-

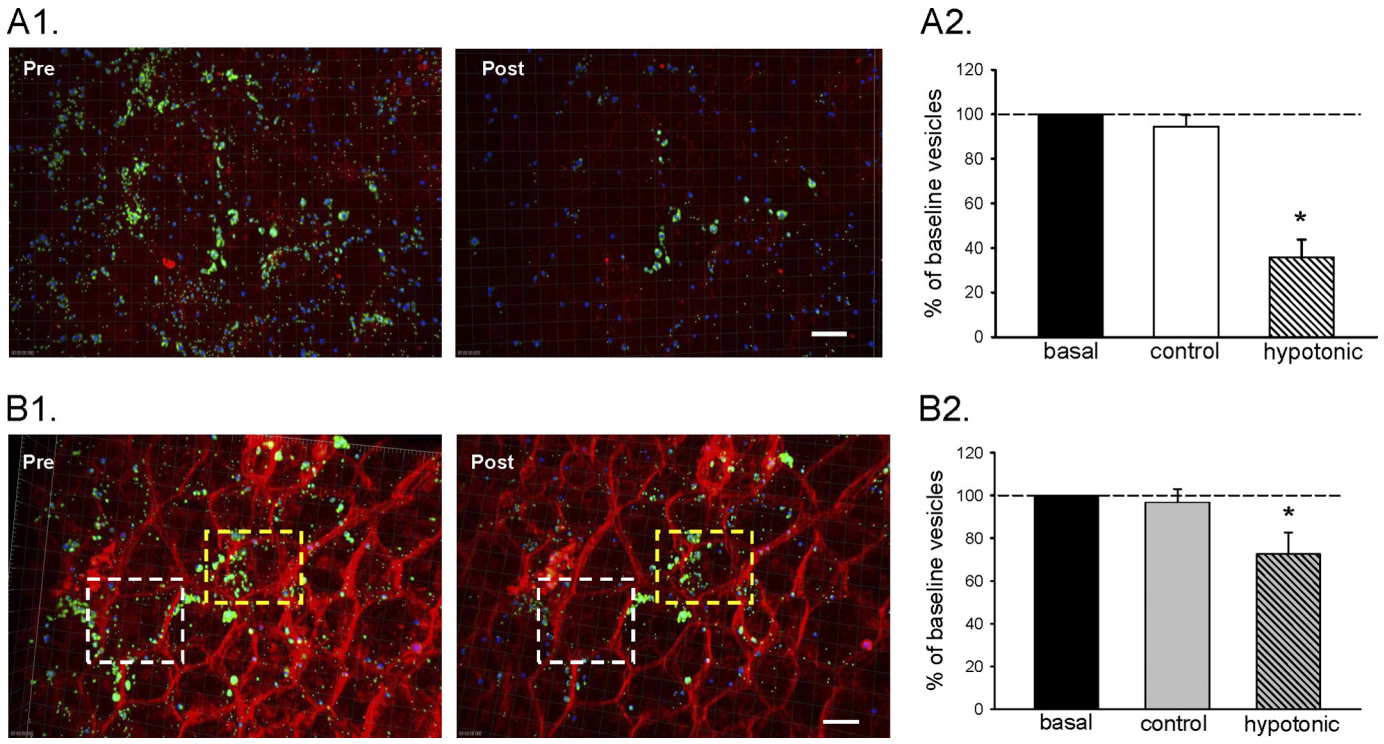

FIGURE 3. **Confocal imaging of confluent polarized small and large mouse cholangiocyte monolayers dually labeled with quinacrine and FM4-64.** Representative MSC and MLC monolayers (*A* and *B*, respectively) were labeled with quinacrine (*green*) and FM4-64 (*red*). A spot detection algorithm was applied to count small (0.4–0.99-μm; *gray spheres*) and large (≥1-μm; *blue spheres*) vesicles during basal conditions and 90 s after hypotonic (33% decrease in osmolality) buffer was applied to the sample. *Scale bar*, 10 μm. *A1*, representative MSC monolayer at base line (*Pre*; *left panel*) and 90 s after exposure to hypotonic solution (*Post*; *right panel*). *A2*, cumulative data (mean ± S.E.) of MSC monolayers demonstrating total vesicles at base line (*basal*; *black bar*) and 90 s after no exposure (*control*; *white bar*) or hypotonic exposure (*hypotonic*; *striped bar*) reported as the percentage of base-line vesicles. Total vesicles decreased in response to hypotonic exposure ($n = 10$ monolayers; *, $p < 0.01$) *versus* control ($n = 10$ monolayers) are shown. *B1*, representative MLC monolayer at base line (*Pre*) and 90 s after (*Post*) exposure to hypotonic buffer. Note that the loss of quinacrine vesicles is not uniform among all cells of the monolayer. A representative responding cell (defined as a loss of ≥5% of total vesicles) and a non-responding cell are outlined in *white* and *yellow boxes*, respectively. *B2*, cumulative data (mean ± S.E.) of MLC monolayers demonstrating total vesicles at base line (*basal*; *black bar*) and 90 s after no exposure (*control*; *gray bar*) or hypotonic exposure (*hypotonic*; *striped bar*) reported as the percentage of base-line vesicles. Total vesicles decreased in response to hypotonic exposure ($n = 9$; *, $p < 0.01$) *versus* control ($n = 10$).

mately 50% of the cells in a confluent population respond as shown by the representative example in Fig. 3*B* where 23 of 41 MLCs responded to the hypotonic stimulus with a decrease in quinacrine-stained vesicles. These studies demonstrate that staining biliary epithelial cells with quinacrine, a dye with high affinity for ATP, reveals a distinct punctate distribution of fluorescence consistent with ATP-enriched vesicles. The loss of quinacrine vesicles following hypotonic exposure is most consistent with fusion of vesicles and release of quinacrine (and ATP) during exocytosis.

Identification of Distinct Populations of ATP-containing Vesicles in Single Cells—Previous studies of rat cholangiocytes have demonstrated the existence of a pool of small (<1-μm) submembrane vesicles that exhibit rapid recycling (36). To determine whether a fraction of these small vesicles represent the quinacrine/ATP vesicles in human and mouse biliary cells, further analysis of single responding cells (defined as a loss of ≥5% of total vesicles) was performed at higher magnification using digital three-dimensional reconstruction of spinning disk confocal z-stacks. A representative Mz-Cha-1 cell is shown in Fig. 4. The plasma membrane is shown in *red* (FM4-64), and vesicles are shown in *green* (quinacrine). Vesicles were grouped into two categories: small vesicles (0.4–0.99 μm; shown by *gray* marker) and large vesicles (≥1.0 μm; shown by *blue* marker). Following exposure to hypotonic medium (33% decrease in osmolality), the total number of quinacrine vesicles decreased by 41 ± 7%, representing a decrease of 65 ± 5% of small ($p < 0.01$) and a decrease of 17 ± 6% of large ($p < 0.01$) vesicle populations *versus* control cells ($n = 11$ each). The loss of small vesicles was significantly greater than the loss of large vesicles following volume stimulation ($p < 0.01$). The preferential loss of small vesicles was also observed in MSCs and MLCs (Fig. 4*C*). Thus, there are distinct populations of quinacrine vesicles, which can be distinguished based on size and functional response to increases in cell volume.

Visualization of Single Exocytic Events by TIRF Microscopy—To confirm that the observed loss of the small (<1-μm) quinacrine-labeled vesicles in response to cell swelling is due to vesicle fusion and exocytic release, the submembrane space (~100 nm) of single Mz-Cha-1 cells was visualized utilizing TIRF microscopy. Real time analysis of the small vesicles revealed that they are not static but vacillate in a Brownian manner during basal conditions. In some cases, vesicles moved toward the membrane and demonstrated a transient increase in fluorescence intensity followed by a rapid disappearance (Fig. 5). This transient increase in intensity is consistent with exocytic release of quinacrine/ATP into the extracellular space as observed in other cell types (24). Under basal conditions, these release events occurred spontaneously at a rate of 0.9 ± 0.3 events/cell/min (Fig. 5*B*). Increases in cell volume (33%

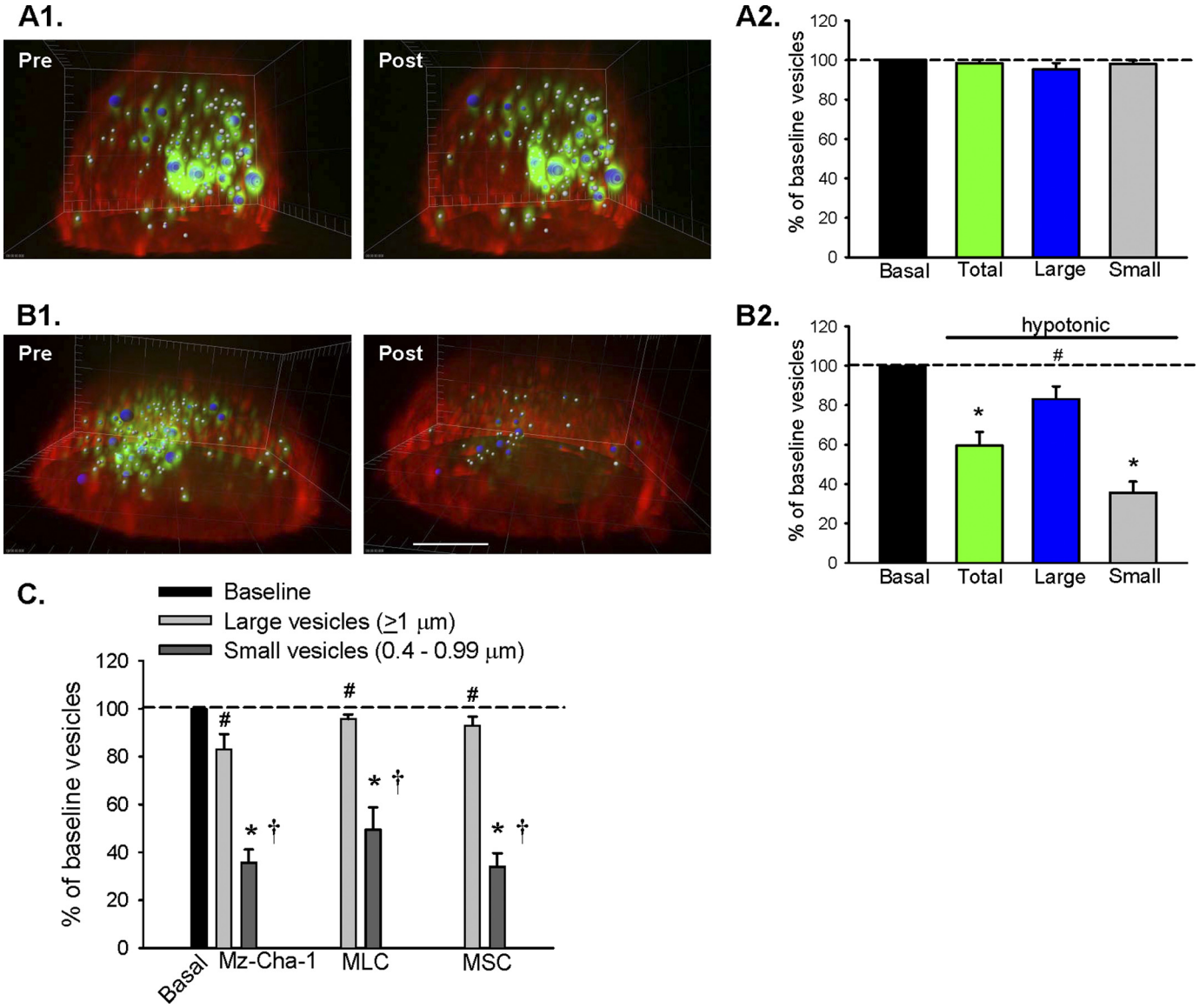

FIGURE 4. **Confocal imaging and three-dimensional reconstruction of single Mz-Cha-1 cells dually labeled with quinacrine and FM4-64.** A spot detection algorithm was applied to count small (0.4–0.99-μm; *gray spheres*) and large (≥1-μm; *blue spheres*) vesicles during basal and stimulated conditions as indicated. *A1*, representative cell imaged at base line (*Pre*) and 90 s later (*Post*) in the absence of any stimulus, demonstrating that the laser does not cause nonspecific photobleaching during the time course of these studies. *A2*, cumulative data (mean ± S.E.) of cells imaged at base line and 90 s later in the absence of any stimulus, demonstrating no effect of photobleaching on total (*green*), large (*blue*), and small (*gray*) quinacrine-stained vesicles *versus* basal (*black*) conditions ($n = 10$, p = not significant). *B1*, representative cell at base line (*left panel*; *Pre*) and 90 s after hypotonic stimulation (33% decrease in osmolality; *right panel*; *Post*). *Scale bar* = 10 μm. *B2*, cumulative data of responding cells (defined as loss of ≥5% of total vesicles) at base line and following hypotonic exposure ($n = 11$). Values represent the percentage of base-line vesicles (mean ± S.E.) for total (*green*), large (*blue*), and small (*gray*) vesicle populations. *, $p < 0.01$; #, $p < 0.05$ *versus* base-line vesicles. *C*, comparison of small and large vesicle populations among Mz-Cha-1, MLC, and MSC cells. Cumulative data of responding cells (defined as loss of ≥5% of total vesicles) and reported as the percentage of basal vesicles. Changes in small (0.4–0.99-μm; *dark gray bar*) and large (≥1-μm; *light gray bar*) vesicle populations were assessed at base line (*black bar*) and 90 s after hypotonic (33% dilution) stimulation. *, $p < 0.001$ *versus* base line; #, $p < 0.05$ *versus* base line; †, $p < 0.01$ small *versus* large vesicles following hypotonic exposure. Values represent mean ± S.E.

decrease in osmolality) increased the rate to 2.8 ± 0.5 events/cell/min ($n = 21$, $p < 0.01$ *versus* basal rate; Fig. 5*B*). These events are most consistent with vesicle fusion and release of quinacrine and other vesicle contents during exocytosis.

ATP Vesicle Formation Is Dependent on SLC17A9—Recently, a vesicular nucleotide transporter, SLC17A9, has been identified (25) and is responsible for loading ATP into vesicles in PC12 cells (25), Jurkat cells (27), and zymogen granules of pancreatic acini (26). Studies were conducted to determine whether SLC17A9 is expressed in biliary epithelial cells and contributes to quinacrine vesicle formation. To evaluate the molecular expression of SLC17A9 in biliary epithelial cells, cDNAs were probed with specific oligonucleotide primers (shown in supplemental Table S1) and amplified using RT-PCR. In Mz-Cha-1, MLC, and MSC cells, clear bands corresponding to SLC17A9 are present (25, 27) (Fig. 6). Next, functional studies were performed to assess the effects of transfection with SLC17A9 siRNA on the number of quinacrine vesicles and on the magnitude of ATP release. As shown in Fig. 6*B*, transfection of Mz-Cha-1 cells with SLC17A9 siRNA decreased SLC17A9 expression by 60 ± 19% ($n = 4$, $p < 0.05$). The decrease in SLC17A9 expression was accompanied by a

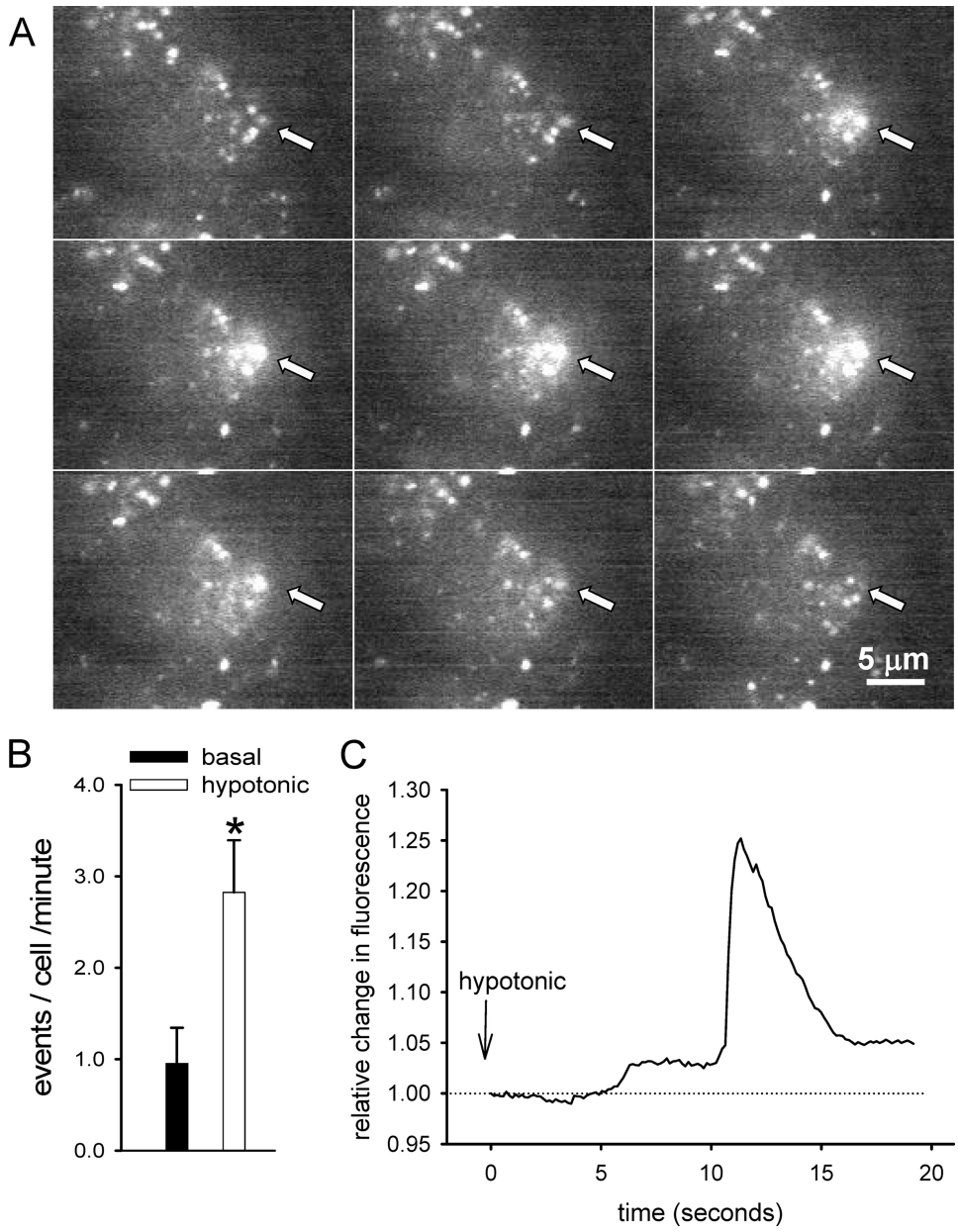

FIGURE 5. **TIRF microscopy reveals population of submembrane quinacrine-rich vesicles.** Mz-Cha-1 cells were loaded with quinacrine, and the submembrane space (to a depth of ~100 nm) was illuminated by the evanescent field generated during TIRF. *A*, time lapse images of a single vesicular exocytic event. The *dotted white line* approximates the plasma membrane of one cell. Quinacrine fluorescence appears in focal areas of high concentration ~1 μm in diameter. In response to hypotonic exposure (33%), vesicles increase in mobility and occasionally fuse with the plasma membrane in a "burst" of fluorescence. These sequential images (from *left* to *right* and from *top* to *bottom*) represent the same cell at 720-ms intervals. The *yellow arrowhead* marks the position of one representative exocytic event in this field of view. In this example, the fluorescence intensity increases sharply, is accompanied by an increase in the diameter of the fluorescent burst, and then rapidly decreases in intensity back to basal levels. *Scale bar*, 5 μm. *B*, cumulative data demonstrating the number of exocytic events per cell imaged during TIRF. The *black bar* represents basal events, and the *white bar* represents events after hypotonic exposure (33% decrease in osmolality) (mean ± S.E. for 21 individual cells each). *, $p < 0.01$ hypotonic *versus* basal. *C*, fluorescence intensity of a single exocytic event was quantified by measuring the relative change in fluorescence intensity over time.

decrease of 37 ± 12% in the total number of quinacrine vesicles compared with mock-transfected cells under basal conditions ($n = 8$, $p < 0.05$). The decrease in total vesicles was due to a decrease in small (<1-μm) vesicles (by 36 ± 11%) as there was no significant change in the number of large (>1-μm) vesicles with SLC17A9 siRNA (Fig. 6, *C* and *D*).

To determine whether the decrease in the number of small vesicles observed with SLC17A9 siRNA affected the magnitude of ATP release, bulk ATP release was measured in near confluent Mz-Cha-1 cells after transfection with SLC17A9 siRNA or mock transfection. As shown in Fig. 7, transfection with SLC17A9 siRNA significantly decreased volume-stimulated ATP release compared with mock-transfected cells ($n = 4$ each, $p < 0.05$; Fig. 7*A*). The ability of SLC17A9 to load vesicles with ATP is dependent on the energy generated by the V-type ATPase (25), and inhibition of the V-type ATPase by bafilomycin A1 (37) impairs storage of ATP in chromaffin granules (38) and secretory granules in astrocytes and mouse splenocytes (21, 27) and abolishes quinacrine vesicle formation and ATP release in rat liver cells (24). To determine whether the V-type ATPase

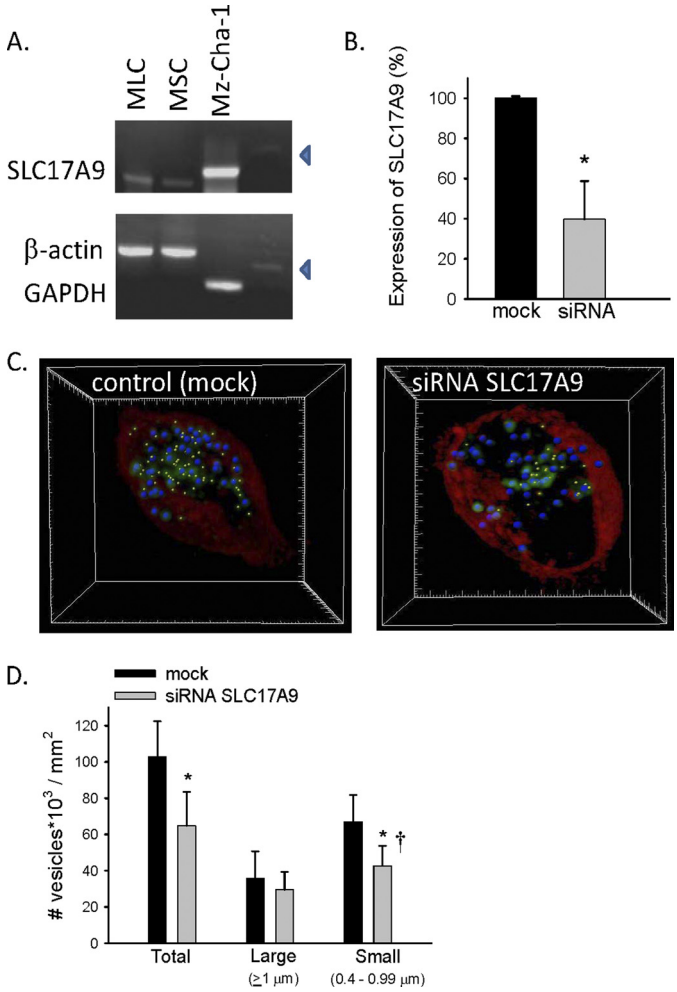

FIGURE 6. **SLC17A9 is expressed by biliary cells and contributes to quinacrine vesicle formation.** *A*, RT-PCR demonstrating expression of SLC17A9 in human Mz-Cha-1, MSC, and MLC cells. Species-specific SLC17A9 primers were used to detect SLC17A9 expression in all models, represented by a band size at 465 bp for human and 397 bp for mouse ("Experimental Procedures"). A λ DNA-HindIII digest ladder was used to delineate the size of respective amplicons; the *arrowhead* represents 564 bp. *B*, cumulative data demonstrating the change in SLC17A9 mRNA levels in cells transfected with non-targeting siRNA (mock), and cells transfected with SLC17A9 siRNA (*, $p < 0.05$ *versus* mock levels). *C*, representative confocal images of Mz-Cha-1 cells dually labeled with quinacrine and FM4-64 and transfected with non-targeting siRNA (mock; *left*) or SLC17A9 siRNA (*right*). A spot detection algorithm was applied to count small (0.4–0.99-μm; *gray spheres*) and large (≥1-μm; *blue spheres*) vesicles during basal conditions. Each square within the grid is 5 × 5 μm. *D*, cumulative data reveal that transfection with SLC17A9 siRNA ($n = 8$; *gray bar*) significantly decreases total and small quinacrine vesicles *versus* mock transfection ($n = 8$; *black bar*) during basal conditions (*, $p < 0.05$). †, $p < 0.05$ small vesicles *versus* large vesicles after transfection of SLC17A9 siRNA. Values represent mean ± S.E.

plays a similar role in biliary cells, bulk ATP release was measured in confluent Mz-Cha-1 cells in the presence or absence of bafilomycin A1. Compared with control cells, bafilomycin significantly blocked volume-stimulated ATP release ($n = 6$ each, $p < 0.01$; Fig. 7*B*). Together, these studies demonstrate that biliary cell ATP release is dependent on the V-type ATPase and the vesicular nucleotide transporter SLC17A9.

Pharmacologic Modulators of Exocytosis Alter Trafficking and Release of Quinacrine Vesicles—Lastly, the effects of pharmacologic modulators of vesicular formation and trafficking were assessed on the number and release of quinacrine vesicles. Studies and analysis were performed in confluent cells to account for differences in individual responding cells. In confluent Mz-Cha-1 cells, incubation with brefeldin A decreased the base-line number of quinacrine-labeled vesicles ($n = 8$, $p < 0.05$; Fig. 8*A1*) and prevented the normal loss of vesicles following hypotonic exposure compared with control cells ($n = 8$ each, $p < 0.05$; Fig. 8*A2*). In contrast, the microtubule-depolymerizing agent nocodazole increased the number of quinacrine-labeled vesicles during basal conditions ($n = 8$ each, $p < 0.01$; Fig. 8*A1*). Following hypotonic exposure, similar to brefeldin, nocodazole prevented the normal loss of quinacrine vesicles ($n = 8$ each, $p < 0.01$; Fig. 8*A2*). Similar findings were observed in MSC and MLC monolayers after incubation with either brefeldin or nocodazole (Fig. 8, *B* and *C*). These results provide a cellular correlate for the effects of these reagents on bulk ATP release, demonstrating that inhibition of ATP release by brefeldin and nocodazole is due to specific effects on the trafficking and release of quinacrine/ATP vesicles.

Regulation of ATP Release and Exocytosis of ATP-enriched Vesicles by PKC—Volume-sensitive ATP release in Mz-Cha-1 cells is accompanied by parallel increases in exocytosis and activation of phorbol-sensitive PKC isoforms (17). To characterize the relationship between PKC and ATP-enriched vesicle formation and release, studies were performed in both MSC and Mz-Cha-1 cells after either acute PKC activation or inhibition. First, exposure to phorbol 12-myristate 13-acetate (PMA) to activate PKC had no effect on basal ATP release but enhanced significantly the amount of ATP released following hypotonic exposure in both MSC and Mz-Cha-1 cells (Fig. 9, *A* and *B*). In contrast, inhibition of PKC by chelerythrine significantly inhibited volume-sensitive ATP release in both cell types. To determine whether the effects of PKC on ATP release were due to effects on the ATP-enriched vesicle fraction, cells were loaded with quinacrine and again visualized by confocal microscopy. Prior exposure to chelerythrine decreased significantly the number of small vesicles at base line and also prevented the normal loss of vesicles in response to hypotonicity (Fig. 9*C*). In additional studies, exposure to PMA had no effect on the basal number of quinacrine-labeled vesicles but significantly increased the number of vesicles lost following hypotonic exposure (Fig. 9*C*). Thus, activation of PKC potentiates the exocytosis of ATP-enriched vesicles in response to cell swelling.

DISCUSSION

In the liver, P2 receptor-mediated signaling has been shown to play important roles in both physiological and pathological conditions, including cell volume regulation (1, 2), proliferation (39), response to injury and fibrosis (40), regulation of portal blood flow (41), and biliary secretion and bile formation (7, 18). Cholangiocyte ATP release is necessary for the initiation of P2 receptor-mediated signaling along intrahepatic bile ducts. Binding of P2 receptors by extracellular nucleotides leads to increases in membrane transport, underlying the mechanism for normal bile dilution and alkalinization (8, 42). Thus, the identification of the mechanism by which biliary epithelial cells release ATP, the initiating step in P2-mediated signaling, is of critical importance to the understanding of normal liver function. Utilizing dynamic multiscale imaging, our studies in

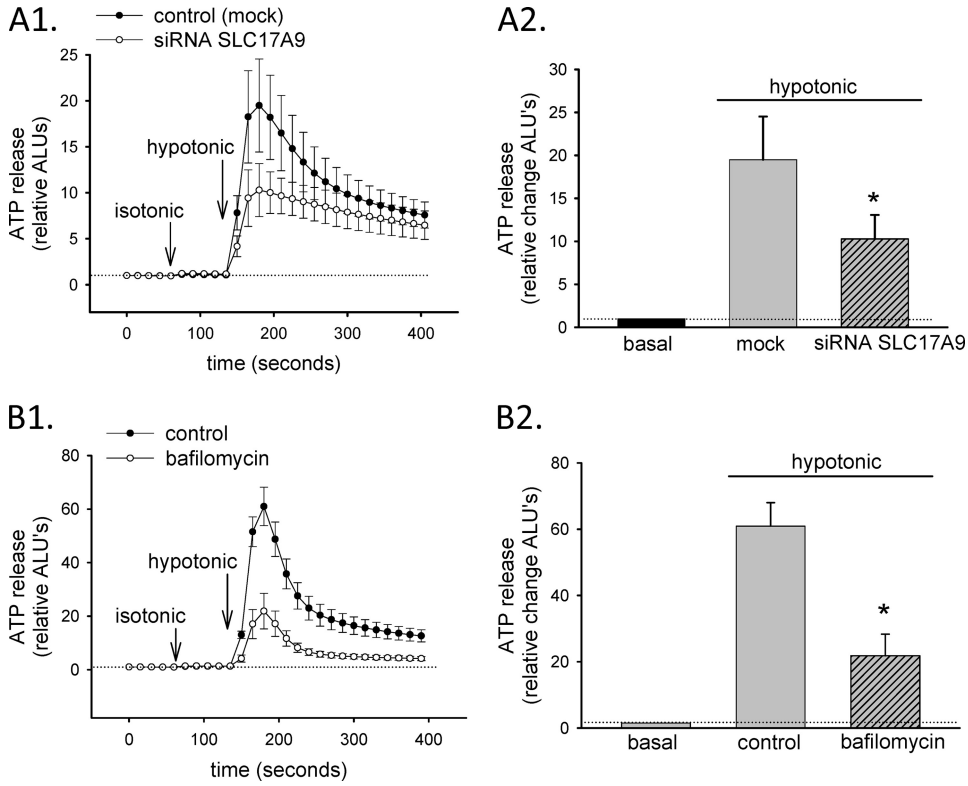

FIGURE 7. **Effects of SLC17A9 siRNA and inhibition of V-type ATPase on ATP release.** Bulk ATP release was detected using a luciferin-luciferase assay and recorded as relative ALUs (*y axis*) from confluent Mz-Cha-1 cells after isotonic and hypotonic exposures (33%). *A1*, representative study demonstrating ATP release from cells transfected with non-targeting siRNA (mock) (●) and cells transfected with SLC17A9 siRNA (○). Addition of isotonic medium (*isotonic*; *arrow*) resulted in a small increase in bioluminescence due to mechanical stimulation. Addition of water to dilute extracellular medium 33% (*hypotonic*; *arrow*) produced a much larger increase in ALUs due to volume-stimulated ATP release. Transfection with SLC17A9 siRNA significantly inhibited volume-stimulated ATP release *versus* mock-transfected cells. *A2*, cumulative data (mean ± S.E.) demonstrating the effect of transfection with SLC17A9 siRNA *versus* mock transfection on volume-stimulated ATP release (*, $p < 0.05$; $n = 4$ each). *B1*, representative study demonstrating ATP release from control cells (●) and cells incubated with bafilomycin (5 μm × 30 min) (○). *B2*, cumulative data (mean ± S.E.) demonstrating the effect of bafilomycin *versus* control on volume-stimulated ATP release (*, $p < 0.01$; $n = 6$ each).

human and mouse biliary cells provide evidence that the mechanism mediating volume-stimulated ATP release is through exocytosis of ATP-enriched vesicles. Evidence for this includes the following. (i) Pharmacologic inhibition of vesicular formation and trafficking blocked ATP release. (ii) ATP release occurred as stochastic, non-recurring point source bursts from individual cells. (iii) ATP stores within cells as demonstrated by quinacrine uptake occurred in distinct vesicles ranging from 0.4 to 1.5 μm in diameter. (iv) ATP-enriched vesicle formation and ATP release were dependent on the vesicular nucleotide transporter SLC17A9 and the V-type ATPase. (v) Fusion and release of vesicle contents in response to increases in cell volume depended on intact microtubules and vesicular trafficking pathways. Together, these findings support an essential role for exocytosis of ATP-enriched vesicles in the initiation of P2 signaling in biliary epithelium.

Since the original description of ATP as a signaling molecule by Burnstock *et al.* (43), studies have focused on identifying the mechanism responsible for cellular ATP release. Although exocytosis of ATP-containing vesicles has been identified as a primary mechanism initiating purinergic signaling in neurons and astrocytes (21, 33, 44), the cellular basis for ATP release in epithelial cells has not been clearly defined. This is especially true for cholangiocytes, which express a number of ATP-binding cassette proteins, including CFTR, implicated in regulated ATP release. To exclude potential effects of CFTR on ATP release, we utilized novel cholangiocyte models derived from the large and small mouse intrahepatic bile ducts which do and do not express CFTR, respectively (29). Significantly, both models contained a population of ATP-enriched vesicles that underwent dynamic changes in trafficking and release in response to mechanosensitive stimulation associated with ATP release.

Cholangiocytes exhibit a rapid rate of constitutive exocytosis under basal conditions that increases dramatically upon stimulation (36). In fact, based on dual measurements of membrane capacitance and FM1-43 fluorescence, cholangiocytes exhibit a constitutive rate of exocytosis equal to 1.4% of the apical membrane surface area/min, and increases in cell volume increase the rate of exocytosis 10-fold (36). This high rate of exocytosis is made possible by the existence of a dense population of vesicles at the submembrane space that undergoes rapid recycling (36). To determine whether a subset of these vesicles represent the ATP-enriched compartment, we loaded cells with quinacrine, which has a high affinity for ATP and has been used to label ATP stores in other cell models (21, 23, 32–34). Labeling of both human and mouse biliary cells revealed a punctate granular pattern consistent with a vesicular origin. Vesicles ranged from 0.4 to 1.5 μm in diameter, and the smaller vesicles (<1 μm) were functionally the most dynamic in response to increases in cell volume. Interestingly, the high rate of consti-

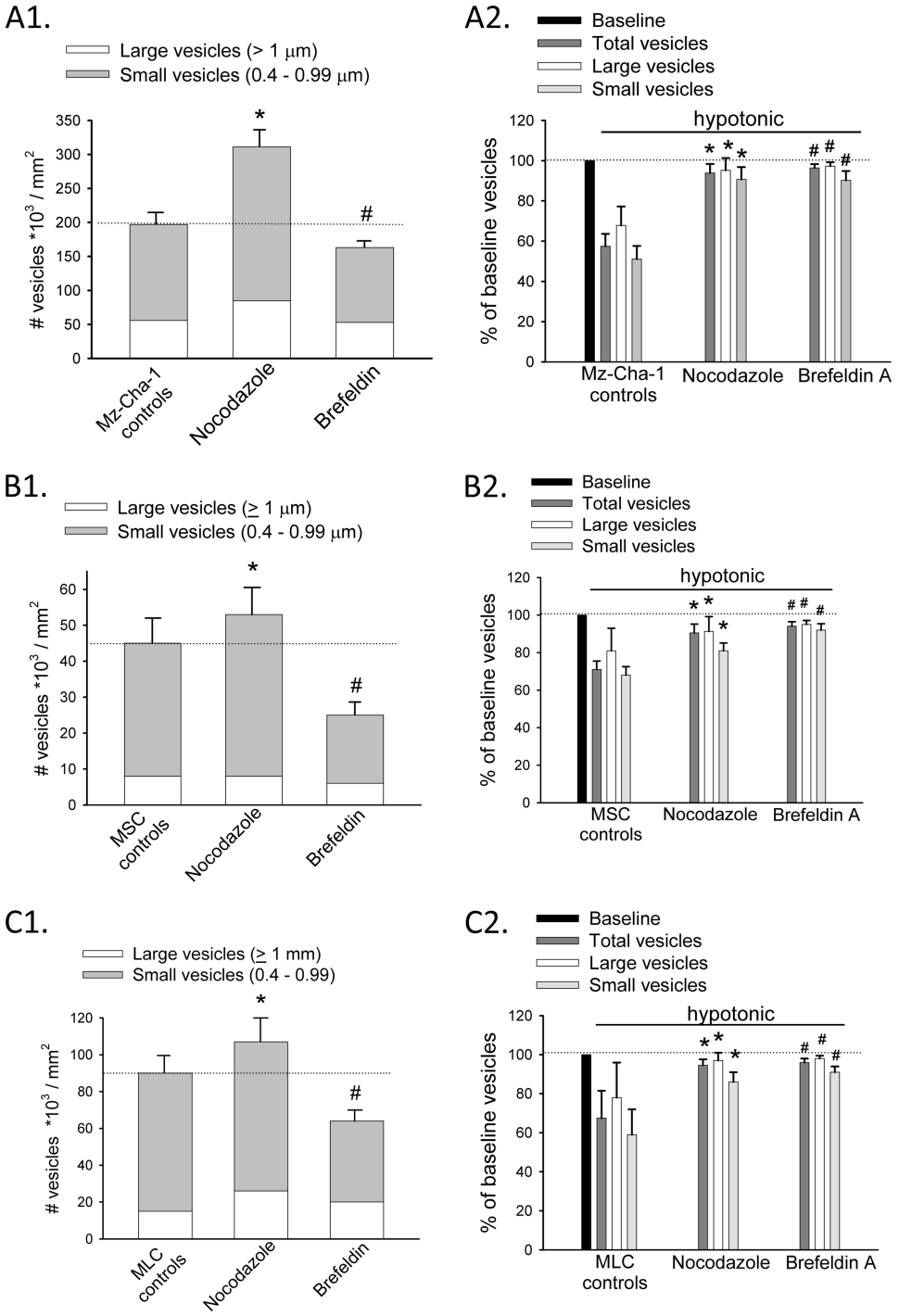

FIGURE 8. **Effects of pharmacologic inhibition of vesicle formation (brefeldin A) and trafficking (nocodazole) on quinacrine vesicles.** Confluent Mz-Cha-1, MSC, and MLC cells were dually labeled with quinacrine and FM4-64 and underwent confocal imaging in the presence or absence of nocodazole (10 μM × 30 min) or brefeldin A (10 μM × 2 h). A spot detection algorithm was applied to count small (0.4–0.99-μm) and large (≥1-μm) vesicles during basal conditions and 90 s after hypotonic exposure (33% decrease in osmolality). *A1*, total number of vesicles for confluent Mz-Cha-1 cells reported as vesicles/mm^2. The *bars* represent total vesicles (mean ± S.E.) and the fraction of large vesicles (*white*) and small vesicles (*gray*) under basal conditions ($n = 8$) and after treatment with nocodazole ($n = 8$) or brefeldin ($n = 8$). *, $p < 0.01$ *versus* control; #, $p < 0.05$ *versus* control. *A2*, cumulative data for Mz-Cha-1 cells demonstrating changes in total (*dark gray bar*), large (*white bar*), and small (*light gray bar*) vesicle populations following hypotonic stimulation in control cells ($n = 8$) and in the presence of nocodazole ($n = 8$) or brefeldin A ($n = 8$) reported as the percentage of base-line vesicles (*black bar*). *, $p < 0.01$ *versus* control; #, $p < 0.05$ *versus* control. *B1*, total number of vesicles for confluent MSC monolayers reported similarly to Mz-Cha-1 cells above under basal conditions ($n = 10$) and after treatment with nocodazole ($n = 7$) or brefeldin ($n = 9$). *, $p < 0.01$ *versus* control; #, $p < 0.05$ *versus* control. *B2*, cumulative data (mean ± S.E.) for MSC monolayers demonstrating changes in vesicle populations following hypotonic stimulation in control cells ($n = 10$) and in the presence of nocodazole ($n = 7$) or brefeldin A ($n = 9$) reported as the percentage of base-line vesicles. *, $p < 0.01$ *versus* control; #, $p < 0.05$ *versus* control. *C1*, total number of vesicles for confluent MLC monolayers under basal conditions ($n = 8$) and after treatment with nocodazole ($n = 7$) or brefeldin ($n = 7$). *, $p < 0.01$ *versus* control; #, $p < 0.05$ *versus* control. *C2*, cumulative data (mean ± S.E.) for MLC monolayers demonstrating changes in vesicle populations following hypotonic stimulation in control cells ($n = 8$) and in the presence of nocodazole ($n = 7$) or brefeldin A ($n = 7$) reported as the percentage of base-line vesicles. *, $p < 0.01$ *versus* control; #, $p < 0.05$ *versus* control.

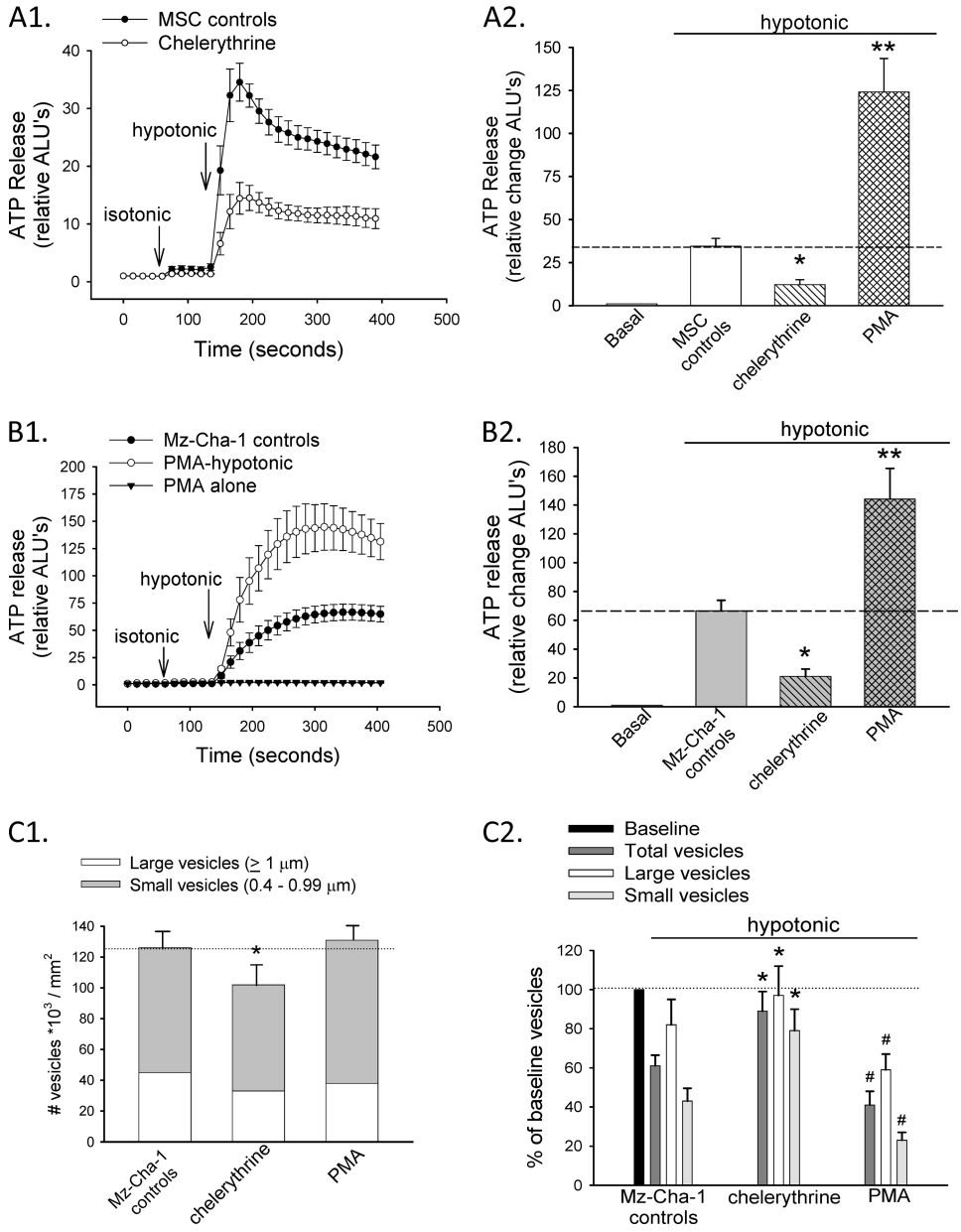

FIGURE 9. **Regulation of ATP release and exocytosis of ATP-enriched vesicles by PKC.** Bulk ATP release (ALUs) was measured from confluent MSC (*A1*) and Mz-Cha-1 (*B1*) cells after isotonic and hypotonic (33%) exposures in control conditions or after incubation with chelerythrine (20 μm × 15 min) or PMA (1 μm × 10 min). *A2* and *B2*, cumulative data demonstrating the effects of PKC stimulation by PMA or inhibition by chelerythrine on hypotonic solution-stimulated ATP release. Data represent the mean ± S.E. of maximal ATP release (n = 6–8 for each). *, hypotonic-stimulated ATP release was significantly decreased by chelerythrine, $p < 0.05$ *versus* control; **, hypotonic-stimulated ATP release was significantly increased by PMA, $p < 0.01$ *versus* control. *C*, Mz-Cha-1 cells were labeled with quinacrine and imaged via confocal microscopy according to the protocol in Fig. 3. *C1*, total number of vesicles for confluent Mz-Cha-1 cells reported as vesicles/mm^2. The *bars* represent total vesicles (mean ± S.E.) and the fraction of large vesicles (*white*) and small vesicles (*gray*) under basal conditions (n = 10) or after treatment with chelerythrine (n = 6) or PMA (n = 8). *, $p < 0.01$ *versus* control. *C2*, cumulative data for Mz-Cha-1 cells demonstrating changes in total (*dark gray bar*), large (*white bar*), and small (*light gray bar*) vesicle populations following hypotonic stimulation in control cells (n = 8) and in the presence of chelerythrine (n = 6) or PMA (n = 8) reported as the percentage of base-line vesicles (*black bar*). *, $p < 0.01$ *versus* control; #, $p < 0.05$ *versus* control.

tutive exocytosis previously observed in normal rat cholangiocytes is predominantly due to rapid recycling of small (<150-nm) vesicles (36). Utilizing pharmacologic, molecular, and dynamic imaging approaches, we demonstrated parallel regulation of quinacrine-labeled vesicles and bulk ATP release and have presented evidence linking the small (<1-μm) quinacrine-labeled vesicles to the ATP-enriched fraction responsible for the initiation of P2 receptor-mediated signaling.

In response to volume stimulation, all biliary cells exhibited a greater loss of small (<1-μm) *versus* large (>1-μm) vesicles. As we did not utilize specific molecular markers, the origin of these vesicle populations cannot be determined. The larger vesicles may represent lysosomes, which have also been associated with exocytic ATP release (45). However, we did not observe any co-localization of FM4-64-labeled endosomes with quinacrine during the time course of these studies, making recycling and ATP loading into endosomes an unlikely source for the quinacrine/ATP vesicle population. Interestingly, silencing of the vesicular nucleotide transporter SLC17A9 resulted in a significantly greater loss of small *versus* large vesicles, providing fur-

ther evidence of both functional and morphologic differences between these vesicle populations.

These studies represent the first identification and functional characterization of the vesicular nucleotide transporter protein SLC17A9 in biliary cells. SLC17A9 is a 430-amino acid protein with 12 putative transmembrane domains and with the exception of some variability in the NH_2 region is relatively conserved among species (25). We have now shown that SLC17A9 is responsible for the formation of ATP vesicles in biliary cells consistent with findings in PC12 cells (25), Jurkat cells (27), and pancreatic acinar cells (26). The mechanism by which SLC17A9 transports ATP into vesicles is far from understood but relies on generation of a $\Delta\Psi$, an electrical potential, across the vesicle membrane through action of the V-type ATPase (25). Inhibition of the V-type ATPase by bafilomycin in the current studies was associated with a marked decrease in ATP release. Loading of ATP into vesicles therefore may be complex but critical for normal epithelial function. Defects in the process may decrease ATP availability for the initiation of purinergic signaling. Thus, a decrease of intracellular ATP stores associated with cholestasis (46) may have important consequences for purinergic receptor-mediated cell and organ functions.

Once formed, vesicles must traffic to the appropriate plasma membrane targets prior to fusion and release. Our current studies demonstrate that microtubule polymerization is critical for ATP vesicle trafficking as the microtubule inhibitor nocodazole trapped quinacrine vesicles intracellularly and inhibited ATP release. How ATP-containing vesicles interact with microtubules is unknown, but PI3K has been shown to be important for organization and stability of vesicle-microtubule interactions (47). This is interesting in light of the finding that the 3-OH lipid products of phosphoinositide 3-kinase regulate ATP release in biliary cells (18). Cholangiocytes also express multiple PKC isoforms, both Ca^{2+}-dependent and atypical, that are differentially regulated in response to various mechanosensitive stimuli, such as cell swelling (19) or shear stress (3), to coordinate cellular ATP release. In other cell types, interactions of PKC, Ca^{2+}, and SNARE proteins coordinate vesicle movement along microtubules and docking with target plasma membrane areas during vesicle fusion (48). The current findings that exocytosis of ATP vesicles was prevented or augmented by inhibition or activation of PKC, respectively, is compatible with a model in which PMA-sensitive PKC isoforms prime a pool of ATP vesicles, increasing fusion and exocytosis upon hypotonic exposure. Thus, cell-to-cell variability in the presence, localization, and activation of PKC isoforms, phosphoinositide 3-kinase, or SNARE complexes may explain differences in ATP release between cell types.

The finding that only a subset of cells release ATP in response to hypotonic exposure is intriguing. Similar observations have been made in astrocytes where only a subset of cells releases ATP (49). As discussed above, differences in the type or activity of protein kinases, intracellular [Ca^{2+}], or the Ca^{2+}-sensing machinery may exist between individual cells and potentially explain observed differences in ATP release between cells in a given population. Given the high concentration of ATP in intracellular vesicles, including an estimated concentration of up to 1 mM in zymogen granules from pancreatic acini (26) for example, release of only a few vesicles among a cell population may account for substantial changes in the extracellular concentration of ATP. In the current studies, point source bursts of released ATP diffused radially ~300 μm, a distance approximating 20 cell diameters. Blocking P2 receptors by suramin did not affect the number of bursts or the diameter of individual burst events, excluding ATP-dependent ATP release (*i.e.* regenerative ATP release) as a mechanism of signal propagation. Each burst represents a single exocytic event, demonstrating that one cell can signal to many surrounding cells. Although speculation, this may ensure dynamic ATP-dependent signaling with minimal loss of total ATP stores at the tissue or organ level. The spatial and temporal aspects of Ca^{2+} signaling initiated by extracellular nucleotides in the regulation of physiological hepatobiliary functions as well as potential perturbations associated with pathologic conditions, such as those associated with cholestasis, deserve further study.

Lastly, these studies do not exclude an additional contribution of membrane ATP transporters or channels to regulated ATP release. In all the biliary models studied, inhibition of vesicular trafficking by pharmacologic agents or anti-SLC17A9 siRNA did not completely eliminate ATP release. Although these findings may be explained by incomplete pharmacologic inhibition or molecular silencing, the possibility of non-vesicular pathways contributing to ATP release cannot be excluded completely. In fact, both channel-mediated and exocytic pathways may be operative in the same cell type. For instance, during vesicle fusion with the plasma membrane, vesicle-bound ATP transporters could be incorporated into the membrane and contribute to ATP efflux. As an additional level of complexity, recent evidence suggests that ATP release pathways may vary in response to different stimuli within the same cell type. For example, human T lymphoma Jurkat cells release ATP via vesicular exocytosis during T cell receptor stimulation (27), whereas these same cells release ATP as a "find me" or "death" signal during apoptosis via pannexin-1 channels (50).

In conclusion, the initiation of P2 receptor-mediated signaling in biliary cells occurs in part via exocytosis of ATP-containing vesicles. Understanding the mechanism by which ATP-enriched vesicles are formed, trafficked, and released will be critical to understanding hepatobiliary functions during health and disease and may suggest targeted therapeutic strategies that modulate extracellular ATP concentrations.

Acknowledgments—MSC and MLC cells were kindly provided by Dr. Gianfranco Alpini, Texas A&M Health Science Center College of Medicine, Temple, TX. TIRF, spinning disk confocal imaging, and three-dimensional volume rendering measurements were carried out in the University of Texas Southwestern Live Cell Imaging Facility.

REFERENCES

1. Feranchak, A. P., Roman, R. M., Schwiebert, E. M., and Fitz, J. G. (1998) *J. Biol. Chem.* **273,** 14906–14911
2. Wang, Y., Roman, R., Lidofsky, S. D., and Fitz, J. G. (1996) *Proc. Natl. Acad. Sci. U.S.A.* **93,** 12020–12025
3. Woo, K., Dutta, A. K., Patel, V., Kresge, C., and Feranchak, A. P. (2008) *J. Physiol.* **586,** 2779–2798
4. Feranchak, A. P., Doctor, R. B., Troetsch, M., Brookman, K., Johnson,

S. M., and Fitz, J. G. (2004) *Gastroenterology* **127,** 903–913
5. Dutta, A. K., Khimji, A. K., Sathe, M., Kresge, C., Parameswara, V., Esser, V., Rockey, D. C., and Feranchak, A. P. (2009) *Am. J. Physiol. Gastrointest. Liver Physiol.* **297,** G1009–G1018
6. Dutta, A. K., Khimji, A. K., Kresge, C., Bugde, A., Dougherty, M., Esser, V., Ueno, Y., Glaser, S. S., Alpini, G., Rockey, D. C., and Feranchak, A. P. (2011) *J. Biol. Chem.* **286,** 766–776
7. Dutta, A. K., Woo, K., Doctor, R. B., Fitz, J. G., and Feranchak, A. P. (2008) *Am. J. Physiol. Gastrointest. Liver Physiol.* **295,** G1004–G1015
8. Feranchak, A. P., and Fitz, J. G. (2002) *Semin. Liver Dis.* **22,** 251–262
9. Minagawa, N., Nagata, J., Shibao, K., Masyuk, A. I., Gomes, D. A., Rodrigues, M. A., Lesage, G., Akiba, Y., Kaunitz, J. D., Ehrlich, B. E., Larusso, N. F., and Nathanson, M. H. (2007) *Gastroenterology* **133,** 1592–1602
10. Feranchak, A. P., and Fitz, J. G. (2007) *Gastroenterology* **133,** 1726–1728
11. Gigliozzi, A., Fraioli, F., Sundaram, P., Lee, J., Mennone, A., Alvaro, D., and Boyer, J. L. (2000) *Gastroenterology* **119,** 1113–1122
12. Cohn, J. A., Strong, T. V., Picciotto, M. R., Nairn, A. C., Collins, F. S., and Fitz, J. G. (1993) *Gastroenterology* **105,** 1857–1864
13. Roman, R. M., Lomri, N., Braunstein, G., Feranchak, A. P., Simeoni, L. A., Davison, A. K., Mechetner, E., Schwiebert, E. M., and Fitz, J. G. (2001) *J. Membr. Biol.* **183,** 165–173
14. Feranchak, A. P., Fitz, J. G., and Roman, R. M. (2000) *J. Hepatol.* **33,** 174–182
15. Reddy, M. M., Quinton, P. M., Haws, C., Wine, J. J., Grygorczyk, R., Tabcharani, J. A., Hanrahan, J. W., Gunderson, K. L., and Kopito, R. R. (1996) *Science* **271,** 1876–1879
16. Watt, W. C., Lazarowski, E. R., and Boucher, R. C. (1998) *J. Biol. Chem.* **273,** 14053–14058
17. Gatof, D., Kilic, G., and Fitz, J. G. (2004) *Am. J. Physiol. Gastrointest. Liver Physiol.* **286,** G538–G546
18. Feranchak, A. P., Roman, R. M., Doctor, R. B., Salter, K. D., Toker, A., and Fitz, J. G. (1999) *J. Biol. Chem.* **274,** 30979–30986
19. Roman, R. M., Bodily, K. O., Wang, Y., Raymond, J. R., and Fitz, J. G. (1998) *Hepatology* **28,** 1073–1080
20. Burnstock, G. (2003) in *Current Topics in Membranes: Extracellular Nucleotides and Nucleosides* (Schwiebert, E. M., ed) pp. 307–368, Academic Press, San Diego, CA
21. Coco, S., Calegari, F., Pravettoni, E., Pozzi, D., Taverna, E., Rosa, P., Matteoli, M., and Verderio, C. (2003) *J. Biol. Chem.* **278,** 1354–1362
22. Maroto, R., and Hamill, O. P. (2001) *J. Biol. Chem.* **276,** 23867–23872
23. Sorensen, C. E., and Novak, I. (2001) *J. Biol. Chem.* **276,** 32925–32932
24. Feranchak, A. P., Lewis, M. A., Kresge, C., Sathe, M., Bugde, A., Luby-Phelps, K., Antich, P. P., and Fitz, J. G. (2010) *J. Biol. Chem.* **285,** 8138–8147
25. Sawada, K., Echigo, N., Juge, N., Miyaji, T., Otsuka, M., Omote, H., Yamamoto, A., and Moriyama, Y. (2008) *Proc. Natl. Acad. Sci. U.S.A.* **105,** 5683–5686
26. Haanes, K. A., and Novak, I. (2010) *Biochem. J.* **429,** 303–311
27. Tokunaga, A., Tsukimoto, M., Harada, H., Moriyama, Y., and Kojima, S. (2010) *J. Biol. Chem.* **285,** 17406–17416
28. Knuth, A., Gabbert, H., Dippold, W., Klein, O., Sachsse, W., Bitter-Suermann, D., Prellwitz, W., and Meyer zum Büschenfelde, K. H. (1985) *J. Hepatol.* **1,** 579–596
29. Glaser, S. S., Gaudio, E., Rao, A., Pierce, L. M., Onori, P., Franchitto, A., Francis, H. L., Dostal, D. E., Venter, J. K., DeMorrow, S., Mancinelli, R., Carpino, G., Alvaro, D., Kopriva, S. E., Savage, J. M., and Alpini, G. D. (2009) *Lab. Invest.* **89,** 456–469
30. Woo, K., Sathe, M., Kresge, C., Esser, V., Ueno, Y., Venter, J., Glaser, S. S., Alpini, G., and Feranchak, A. P. (2010) *Hepatology* **52,** 1819–1828
31. Taylor, A. L., Kudlow, B. A., Marrs, K. L., Gruenert, D. C., Guggino, W. B., and Schwiebert, E. M. (1998) *Am. J. Physiol. Cell Physiol.* **275,** C1391–C1406
32. Irvin, J. L., and Irvin, E. M. (1954) *J. Biol. Chem.* **210,** 45–56
33. Pangrsic, T., Potokar, M., Stenovec, M., Kreft, M., Fabbretti, E., Nistri, A., Pryazhnikov, E., Khiroug, L., Giniatullin, R., and Zorec, R. (2007) *J. Biol. Chem.* **282,** 28749–28758
34. Mitchell, C. H., Carré, D. A., McGlinn, A. M., Stone, R. A., and Civan, M. M. (1998) *Proc. Natl. Acad. Sci. U.S.A.* **95,** 7174–7178
35. Axelrod, D. (1981) *J. Cell Biol.* **89,** 141–145
36. Doctor, R. B., Dahl, R., Fouassier, L., Kilic, G., and Fitz, J. G. (2002) *Am. J. Physiol. Cell Physiol.* **282,** C1042–C1052
37. Bowman, E. J., Siebers, A., and Altendorf, K. (1988) *Proc. Natl. Acad. Sci. U.S.A.* **85,** 7972–7976
38. Bankston, L. A., and Guidotti, G. (1996) *J. Biol. Chem.* **271,** 17132–17138
39. Thevananther, S., Sun, H., Li, D., Arjunan, V., Awad, S. S., Wyllie, S., Zimmerman, T. L., Goss, J. A., and Karpen, S. J. (2004) *Hepatology* **39,** 393–402
40. Yu, J., Sheung, N., Soliman, E. M., Spirli, C., and Dranoff, J. A. (2009) *Am. J. Physiol. Gastrointest. Liver Physiol.* **296,** G563–G571
41. Yang, W., Benjamin, I. S., and Alexander, B. (2001) *Acta Physiol. Scand.* **171,** 413–418
42. Gradilone, S. A., Masyuk, A. I., Splinter, P. L., Banales, J. M., Huang, B. Q., Tietz, P. S., Masyuk, T. V., and Larusso, N. F. (2007) *Proc. Natl. Acad. Sci. U.S.A.* **104,** 19138–19143
43. Burnstock, G., Campbell, G., Satchell, D., and Smythe, A. (1970) *Br. J. Pharmacol.* **40,** 668–688
44. Pankratov, Y., Lalo, U., Verkhratsky, A., and North, R. A. (2006) *Pflugers Arch.* **452,** 589–597
45. Zhang, Z., Chen, G., Zhou, W., Song, A., Xu, T., Luo, Q., Wang, W., Gu, X. S., and Duan, S. (2007) *Nat. Cell Biol.* **9,** 945–953
46. Spivey, J. R., Bronk, S. F., and Gores, G. J. (1993) *J. Clin. Investig.* **92,** 17–24
47. Zhao, Y., Gaidarov, I., and Keen, J. H. (2007) *J. Biol. Chem.* **282,** 1249–1256
48. Morgan, A., Burgoyne, R. D., Barclay, J. W., Craig, T. J., Prescott, G. R., Ciufo, L. F., Evans, G. J., and Graham, M. E. (2005) *Biochem. Soc. Trans.* **33,** 1341–1344
49. Arcuino, G., Lin, J. H., Takano, T., Liu, C., Jiang, L., Gao, Q., Kang, J., and Nedergaard, M. (2002) *Proc. Natl. Acad. Sci. U.S.A.* **99,** 9840–9845
50. Chekeni, F. B., Elliott, M. R., Sandilos, J. K., Walk, S. F., Kinchen, J. M., Lazarowski, E. R., Armstrong, A. J., Penuela, S., Laird, D. W., Salvesen, G. S., Isakson, B. E., Bayliss, D. A., and Ravichandran, K. S. (2010) *Nature* **467,** 863–867